The Plant Cell, Vol. 26: 2601–2616, June 2014, www.plantcell.org 

# The *jiaoyao1* Mutant Is an Allele of *korrigan1* That Abolishes Endoglucanase Activity and Affects the Organization of Both Cellulose Microfibrils and Microtubules in *Arabidopsis*[CW]

**Lei Lei,[a] Tian Zhang,[b,1] Richard Strasser,[c,1] Christopher M. Lee,[d] Martine Gonneau,[e] Lukas Mach,[c] Samantha Vernhettes,[c] Seong H. Kim,[d] Daniel J. Cosgrove,[b] Shundai Li,[a] and Ying Gu[a,2]**

[a] Department of Biochemistry and Molecular Biology, Pennsylvania State University, University Park, Pennsylvania 16802
[b] Department of Biology, Pennsylvania State University, University Park, Pennsylvania 16802
[c] Department of Applied Genetics and Cell Biology, University of Natural Resources and Life Sciences, A-1190 Vienna, Austria
[d] Chemical Engineering and Materials Research Institute, Pennsylvania State University, University Park, Pennsylvania 16802
[e] Institut Jean-Pierre Bourgin, Unité Mixte de Recherche 1318 INRA-AgroParisTech, 78026 Versailles, France

**In higher plants, cellulose is synthesized by plasma membrane–localized cellulose synthase complexes (CSCs). *Arabidopsis thaliana* GH9A1/KORRIGAN1 is a membrane-bound, family 9 glycosyl hydrolase that is important for cellulose synthesis in both primary and secondary cell walls. Most previously identified *korrigan1* mutants show severe phenotypes such as embryo lethality; therefore, the role of GH9A1 in cellulose synthesis remains unclear. Here, we report a novel A577V missense mutation, designated *jiaoyao1* (*jia1*), in the second of the glycosyl hydrolase family 9 active site signature motifs in GH9A1. *jia1* is defective in cell expansion in dark-grown hypocotyls, roots, and adult plants. Consistent with its defect in cell expansion, this mutation in GH9A1 resulted in reduced cellulose content and reduced CSC velocity at the plasma membrane. Green fluorescent protein–GH9A1 is associated with CSCs at multiple locations, including the plasma membrane, Golgi, *trans*-Golgi network, and small CESA-containing compartments or microtubule-associated cellulose synthase compartments, indicating a tight association between GH9A1 and CSCs. GH9A1$^{A577V}$ abolishes the endoglucanase activity of GH9A1 in vitro but does not affect its interaction with CESAs in vitro, suggesting that endoglucanase activity is important for cellulose synthesis. Interestingly, *jia1* results in both cellulose microfibril and microtubule disorganization. Our study establishes the important role of endoglucanase in cellulose synthesis and cellulose microfibril organization in plants.**

## INTRODUCTION

Plant endo-β-1,4-glucanases (EGases) belong to glycosyl hydrolase family 9, which consists of three distinct structural subclasses. *Arabidopsis thaliana* encodes at least 25 EGases, comprising members that are membrane anchored (class A), secreted to the cell wall (class B), or secreted and have a CBM49 carbohydrate binding module (class C) (Urbanowicz et al., 2007). While certain microbial EGases degrade crystalline cellulose, plant EGases are unable to hydrolyze crystalline cellulose. However, endoglucanase activity for class C EGases has been observed with various substrates, including xyloglucan, xylan, glucomannans, mixed-linkage glucans, and soluble cellulose derivatives such as carboxymethyl cellulose (CMC) and noncrystalline phosphoric acid–swollen cellulose (Master et al., 2004; Yoshida et al., 2006; Urbanowicz et al., 2007). *Arabidopsis* GH9A1/KORRIGAN1 (KOR1) belongs to class A type II integral membrane EGases, consisting of a cytoplasmic domain, a single transmembrane domain, and an extracellular catalytic domain. Although AtGH9A1 does not have a CBM domain, it has been shown to hydrolyze CMC and amorphous cellulose in vitro (Mølhøj et al., 2001a; Master et al., 2004; Liebminger et al., 2013). *N*-Glycosylation is important for KOR1 enzymatic activity, as demonstrated for both Ptt-Cel9A, the *Populus tremula* × *tremuloides* KOR1 homolog, and AtGH9A1 (Master et al., 2004; Liebminger et al., 2013).

In *Arabidopsis*, there are three class A EGases: GH9A1, GH9A2, and GH9A3. GH9A1 is ubiquitously expressed, whereas GH9A2 and GH9A3 are expressed in restricted cell types (Mølhøj et al., 2001b). The *kor1* mutants, first identified in a genetic screen for short hypocotyls, display primary cell wall defects such as irregular cell wall separations, abnormal cytokinesis, reduced cellulose content, and inhibition of tissue elongation (Nicol et al., 1998; Zuo et al., 2000; His et al., 2001; Lane et al., 2001; Mølhøj et al., 2001a; Sato et al., 2001). Furthermore, the *irregular xylem2* mutants, identified to be allelic to *kor1*, have a cellulose deficiency specific to the secondary cell wall (Szyjanowicz et al., 2004).

The tomato (*Solanum lycopersicum*) GH9A1 homolog Sl-GH9A1 was localized to both the Golgi and the plasma membrane by Suc gradient fractionation of tomato root microsomal membranes (Brummell et al., 1997). Partially consistent with this observation, AtGH9A1-GFP (for green fluorescent protein) showed a punctate pattern in interphase cells and was observed at the cell plate during cytokinesis of tobacco (*Nicotiana tabacum*) BY2 cells (Zuo et al., 2000). Overexpression of GFP-AtGH9A1 partially rescued

[1] These authors contributed equally to this work.
[2] Address correspondence to yug13@psu.edu.
The author responsible for distribution of materials integral to the findings presented in this article in accordance with the policy described in the Instructions for Authors (www.plantcell.org) is: Ying Gu (yug13@psu.edu).
[C] Some figures in this article are displayed in color online but in black and white in the print edition.
[W] Online version contains Web-only data.
www.plantcell.org/cgi/doi/10.1105/tpc.114.126193

*kor1-1* hypocotyl and root growth phenotypes and was localized to an intracellular compartment composed of the Golgi, early endosomes, and tonoplast, but not to the plasma membrane (Robert et al., 2005). These discrepancies in the subcellular localization of GH9A1 have been met with three proposed functions: (1) recognition and removal of disordered glucan chains in cellulose; (2) generation of short primers upon which cellulose polymerization is initiated; and/or (3) termination of cellulose synthesis (Mølhøj et al., 2001a, 2002; Peng et al., 2002). To address whether GH9A1 interacts with or is an integral part of cellulose synthase complexes (CSCs), coimmunoprecipitation experiments were performed in which it was shown that GH9A1 does not stably interact with either primary (CESA3 or CESA6) or secondary (CESA7 or CESA8) CESAs in detergent-solubilized extracts (Szyjanowicz et al., 2004; Desprez et al., 2007). These results cast doubt on whether GH9A1 and CSCs interact directly; however, GFP-GH9A1 is expressed under the control of its endogenous promoter localized to the plasma membrane and is proposed to be a part of primary CSCs (Crowell et al., 2010).

In a screen for seedlings that displayed a root-swelling phenotype, we identified a missense *kor1* allele that we call *jiaoyao1* (*jia1*), named after a diminutive human race documented in Confucianism. A nucleotide substitution (C to T) in *jia1* resulted in an amino acid substitution (A577V) within the second of its glycosyl hydrolase family 9 active site signature motifs, a sequence that is highly conserved among this family of EGases. The characterization of *jia1* revealed that both cellulose microfibril ordering and cortical microtubule organization are reliant on the function of AtGH9A1.

## RESULTS

### *jia1* Is a *KOR1* Missense Allele

To identify novel factors involved in cellulose biosynthesis, we screened ethyl methanesulfonate–mutagenized *Arabidopsis* seedlings (Columbia-0 [Col-0]) for altered root phenotypes. Approximately 100,000 ethyl methanesulfonate–mutagenized seedlings were screened on half-strength Murashige and Skoog (MS) medium supplemented with 1% Suc. Seedlings with short and swollen roots were rescued and their progeny were retested. We identified 15 mutant alleles, which we designated *jia*. All *jia* mutants were recessive, following a 3:1 wild type:*jia* segregation pattern in the F2 generation of an outcross with the wild type. Allelic tests with known cellulose-deficient mutants, such as *kor1* (*rsw2-1*, *kor1-3*), *procuste1* ($cesa6^{prc1-1}$), $cesa3^{je5}$, $cobra^{cob1-4}$, and $cesa1^{rsw1}$, revealed that two *jia1* mutant alleles (*jia1-1* and *jia1-2*) were allelic to $kor1^{kor1-3}$. Although independent isolates, sequencing of the *Arabidopsis GH9A1/KOR1* gene in the corresponding *jia* alleles showed that both contained the identical nucleotide substitution (C to T) in *GH9A1*, which resulted in the amino acid substitution A577V in GH9A1. The *jia1-1* mutant phenotype was rescued by a construct containing the coding region of wild-type GH9A1 driven by its native promoter (Supplemental Figure 1A). The allelism of *jia1* and *kor1* was further supported by partial phenotypic complementation of *jia1-1* by *kor1-3* (Supplemental Figure 1B). Alignment of GH9A1 from monocot, dicot, moss, and green alga species indicated that residue Ala-577 is conserved between various plant species (Supplemental Figure 2).

### *jia1* Shows Defects in Cell Expansion

*jia1-1* mutants exhibited short and swollen seedling roots. Seven-day-old, light-grown *jia1-1* roots were ~67% shorter and ~23% wider than wild-type roots (Figures 1A, 1B, 1D, and 1E). Hypocotyls of dark-grown *jia1-1* mutants were ~40% shorter than those of wild-type plants (Figures 1C and 1F). Additionally, adult *jia1-1* mutants were dwarfed and had shorter siliques and smaller rosette leaves than wild-type plants (Supplemental Figure 3).

To assess the effect of the *jia1* mutation on cellulose synthesis, we quantified the hypocotyl length of 5-d-old, dark-grown mutant and wild-type seedlings and the primary root length of 7-d-old, light-grown mutant and wild-type seedlings on increasing concentrations of the cellulose synthesis inhibitor isoxaben (Scheible et al., 2001; Desprez et al., 2002). We found that *jia1-1* seedlings were hypersensitive to isoxaben as compared with the wild type (Figures 1G and 1H), suggesting that *jia1-1* may be defective in cellulose biosynthesis. Crystalline cellulose analysis using the Updegraff method (Updegraff, 1969) showed that dark-grown hypocotyls of *jia1-1* had ~22% less cellulose than those of the wild type (Figure 1I). The isoxaben hypersensitivity and reduced crystalline cellulose are consistent with the anisotropic growth defects observed for *jia1-1* seedlings (Figures 1C and 1F).

### GH9A1 Colocalizes with CSCs

To examine the subcellular localization of GH9A1, a *ProGH9A1:GFP-GH9A1* construct containing ~2 kb of native *GH9A1* promoter, the coding sequence of *GH9A1*, and an N-terminal GFP tag was transformed into *kor1-3* plants (Paredez et al., 2008). GFP-GH9A1 fully rescued the *kor1-3* mutant phenotype of 7-d-old, light-grown seedlings (Figures 2A and 2B), suggesting that the GFP-GH9A1 fusion protein was functional in plants. In dark-grown hypocotyls, GFP-GH9A1 localized to the plasma membrane with a punctate distribution and to larger intracellular compartments (Figure 2C; Supplemental Movie 1). Time-series imaging showed that plasma membrane–localized GFP-GH9A1 moved bidirectionally and followed linear tracks over time (Figure 2C; Supplemental Movie 1). The average velocity of membrane particles was 343 ± 133 nm/min (range, 0 to 700 nm/min; $n$ = 1167 particles), which is similar to what has been reported previously for CSCs and proteins associated with CSCs (Paredez et al., 2006; Desprez et al., 2007; Gutierrez et al., 2009; Gu et al., 2010; Bischoff et al., 2011; Li et al., 2012).

To examine whether GH9A1 associates with CSCs in vivo, we generated a line expressing both mCherry-CESA3 and GFP-GH9A1. Two-channel confocal imaging revealed that the GFP-GH9A1 signal overlapped extensively with mCherry-CESA3 at the plasma membrane (Figure 3A; Supplemental Movie 2). GFP-GH9A1 and mCherry-CESA3 particles moved along linear tracks, as shown by time-averaged projections of 61 frames from a 5-min time series of images (Figure 3A; Supplemental Movie 2). The linear tracks traveled by mCherry-CESA3 coincided with those of GFP-GH9A1, as shown by the merged image (Figure 3A). Similar to mCherry-CESA3, GFP-GH9A1 particles traveled bidirectionally, and the average velocity of GFP-GH9A1 particles (260 ± 113 nm/min) was similar to that of mCherry-CESA3 particles (268 ± 119 nm/min; $n$ = 671 particles for both signals) in the same cells (Figure 3B).

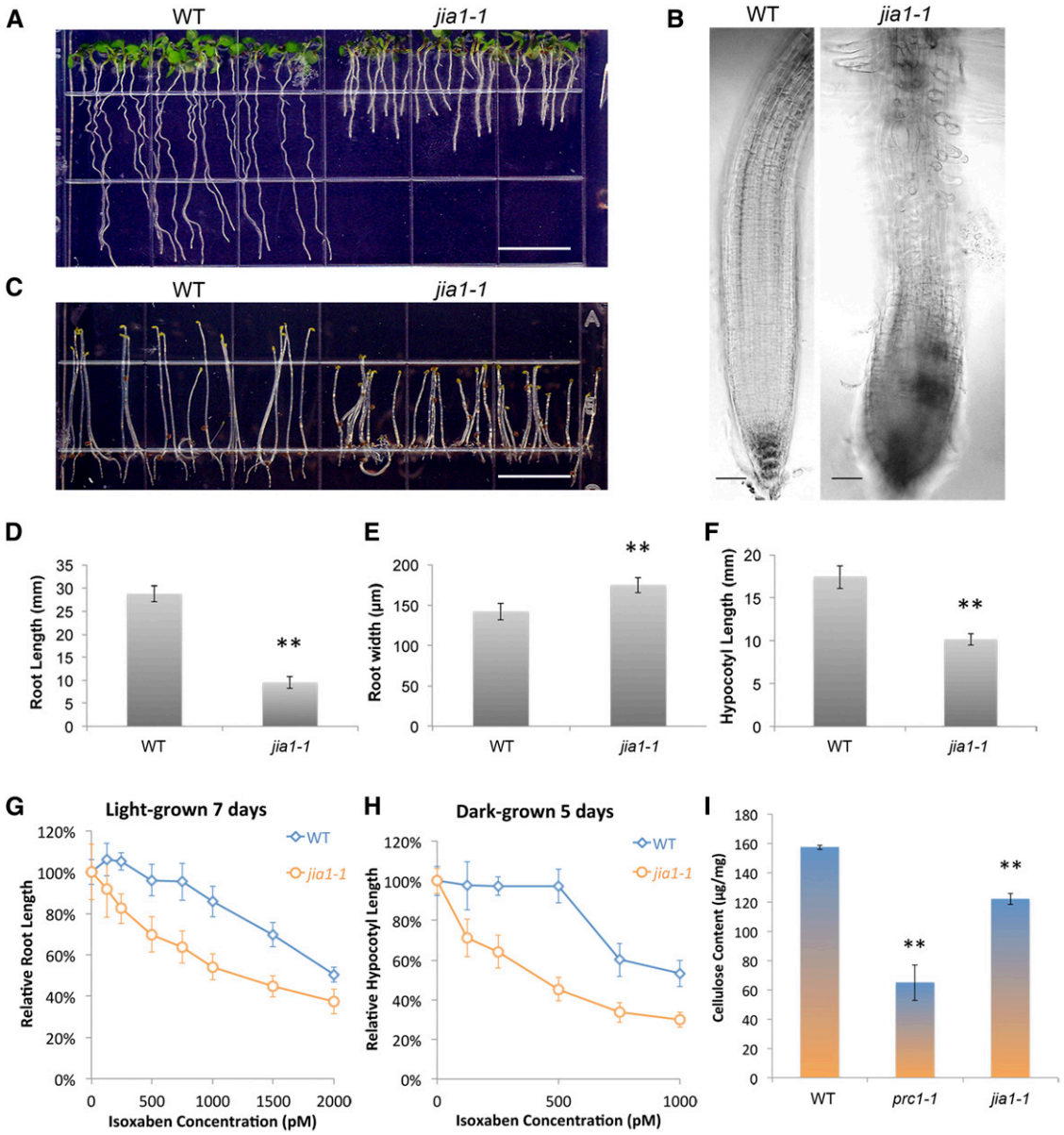


**Figure 1.** *jia1-1* Seedlings Exhibit Aberrant Growth in Both Light-Grown Roots and Dark-Grown Hypocotyls.

**(A)** Seven-day-old, light-grown seedlings of the Col-0 wild type and *jia1-1*. Bar = 1 cm.
**(B)** Primary roots of 7-d-old, light-grown seedlings of the wild type and *jia1-1*. Bars = 50 μm.
**(C)** Five-day-old, dark-grown seedlings of the wild type and *jia1-1*. Bar = 1 cm.
**(D)** and **(E)** Quantification of root length **(D)** and width **(E)** of light-grown wild type and *jia1-1* plants.
**(F)** Quantification of hypocotyl length of dark-grown wild-type and *jia1-1* plants.
In **(D)** to **(F)**, $n \approx 50$ seedlings per genotype. Double asterisks indicate significant differences from the wild type at the same data point ($P < 0.01$, Student's *t* test).
**(G)** and **(H)** *jia1-1* is hypersensitive to the cellulose synthesis inhibitor isoxaben. Seedlings were grown vertically for the indicated number of days on solid MS plates supplemented with increasing concentrations of isoxaben. The effect of isoxaben on primary root length of 7-d-old, light-grown wild-type and *jia1-1* plants **(G)** and the hypocotyl length of 5-d-old, dark-grown wild-type and *jia1-1* plants **(H)** were quantified. $n \approx 50$ seedlings per genotype.
**(I)** Crystalline cellulose content of 4-d-old, dark-grown wild-type (Col-0), *prc1-1*, and *jia1-1* plants. Double asterisks indicate significant differences from the wild type at the same data point ($P < 0.01$, Student's *t* test). Data were collected from five technical replicates for each tissue sample. Error bars represent SD.
[See online article for color version of this figure.]

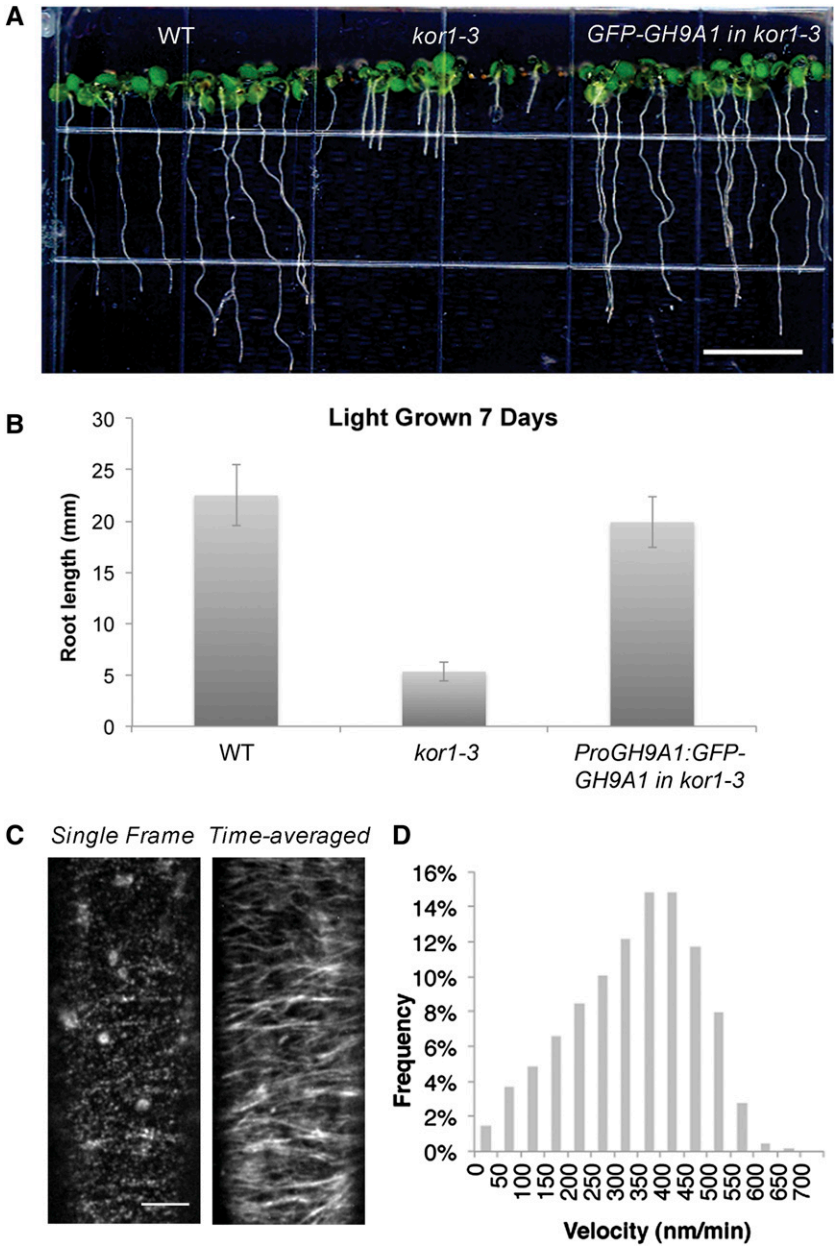


**Figure 2.** GH9A1 Localizes to Distinct Particles at the Plasma Membrane.

**(A)** Seven-day-old, light-grown seedlings of the wild type, *kor1-3*, and *ProGH9A1:GH9A1*-rescued *kor1-3*.
**(B)** Quantification of primary root length of 7-d-old, light-grown wild-type, *kor1-3*, and *ProGH9A1:GH9A1*-rescued *kor1-3* plants. *n* = 60 to 70 seedlings per genotype.
**(C)** Optical sections of epidermal cells in 3-d-old, dark-grown hypocotyls expressing GFP-GH9A1-rescued *kor1-3*. Time-averaged images show linear tracks of GFP-GH9A1. Bar = 5 μm.
**(D)** Histogram of GFP-GH9A1 particle velocities. The mean velocity is 343 ± 133 nm/min (*n* = 1167 particles).
[See online article for color version of this figure.]

These observed velocities for both mCherry-CESA3 and GFP-GH9A1 were lower than what had been observed for either CESA3 or GH9A1 alone (Figure 2D), possibly due to the effect of multiple tags on the motility of CSCs. Nevertheless, the frequency distribution of velocities for mCherryCESA3 was similar to that of GFP-GH9A1 (Figure 3B), further supporting the dynamic similarity of these two molecular components.

CSCs were observed in various cellular locations, including the plasma membrane, the periphery of the Golgi apparatus, and small CESA-containing compartments (SmaCCs) or microtubule-

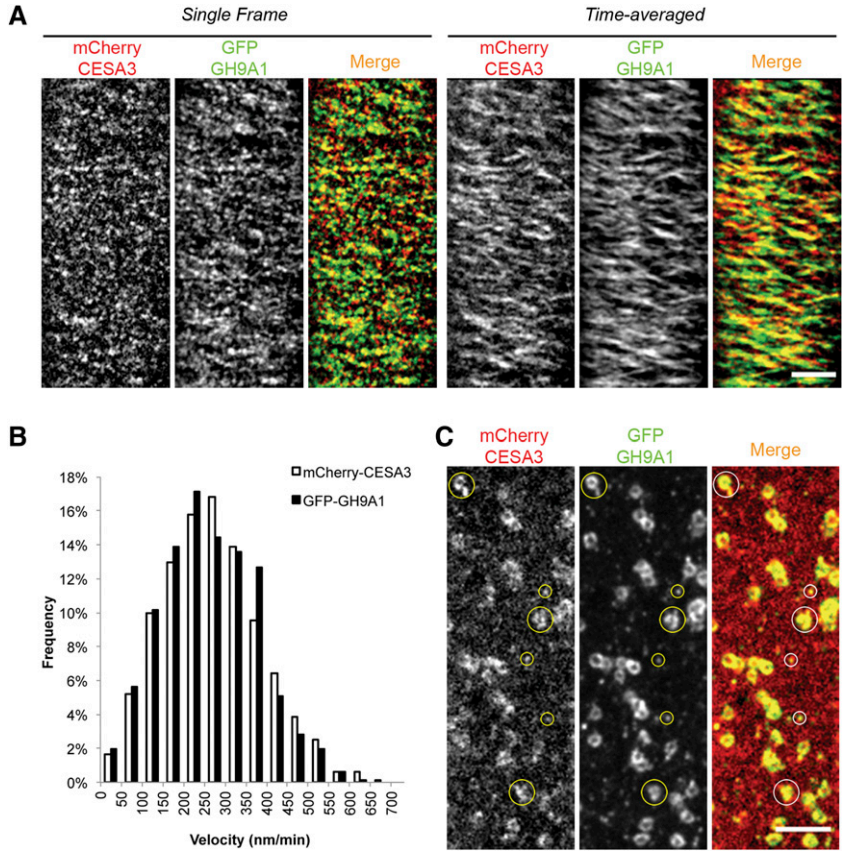


**Figure 3.** GH9A1 Colocalizes with CESA.

*Arabidopsis* seedlings expressing both mCherry-CESA3 and GFP-GH9A1 were grown in the dark for 3 d before imaging.
**(A)** Single optical sections and time averages of 61 frames (5-min duration in 5-s intervals) of plasma membrane–localized mCherry-CESA3 and GFP-GH9A1. The mCherry channel, GFP channel, and merged image of mCherry and GFP are shown. Bar = 5 μm.
**(B)** Histogram of particle velocities. The mean velocity is 268 ± 119 nm/min for mCherry-CESA3 and 260 ± 113 nm/min for GFP-GH9A1 ($n$ = 671 particles for both).
**(C)** Single optical sections of mCherry-CESA3 and GFP-GH9A1 in intracellular compartments after a 2-h exposure to 100 nM isoxaben. Large circles denote Golgi compartments, and small circles denote SmaCCs/MASCs. Bar = 5 μm.
[See online article for color version of this figure.]

associated cellulose synthase compartments (MASCs) (Haigler and Brown, 1986; Crowell et al., 2009; Gutierrez et al., 2009). Isoxaben treatment is known to deplete CSCs from the plasma membrane, with the subsequent appearance of numerous SmaCCs/MASCs (Crowell et al., 2009; Gutierrez et al., 2009). After dark-grown hypocotyls were treated with 100 nM isoxaben for 2 h, GFP-GH9A1 punctae moved simultaneously with SmaCCs/MASCs that were colabeled with mCherry-CESA3 (Figure 3C; Supplemental Movie 3). In addition to SmaCCs/MASCs, GFP-GH9A1 also localized to donut-shaped intracellular compartments that exhibited cytoplasmic streaming and colocalized with mCherry-CESA3 (Figure 3C; Supplemental Movie 3); thus, we predict their identity to be Golgi bodies. These results suggest that GH9A1 associates with primary CSCs at the plasma membrane and various intracellular compartments.

To further examine the identity of the GH9A1-labeled intracellular compartments, we crossed GFP-GH9A1 to a subset of *Arabidopsis* mCherry-labeled organelle marker lines (Geldner et al., 2009). Two putative markers for the Golgi apparatus and the *trans*-Golgi network, mCherry-SYP32 and mCherry-SYP61, respectively, show significant overlap with GFP-GH9A1 (Supplemental Figures 4A and 4B). Similar to structures positive for these Golgi markers, GFP-GH9A1 displayed rapid, nonlinear cytoplasmic streaming (Supplemental Movie 4). Partial colocalization was observed between GFP-GH9A1 and mCherry-VTI12, a putative early endosome/*trans*-Golgi network marker (Uemura et al., 2004). Most often, mCherry-VTI12 was found to label the center of a Golgi stack surrounded by GFP-GH9A1 signal at the periphery (Supplemental Figure 4C). Some small compartments labeled by mCherry-VTI12 were not colocalized with GFP-GH9A1. Signals from GFP-GH9A1 and the post-Golgi/endosome marker mCherry-RabC1 partially overlapped (Supplemental Figure 4D), while GFP-GH9A1 did not colocalize with the endosome/recycling endosome marker mCherry-RabA1g or the late endosome/vacuole

marker mCherry-RabG3f. These results suggest that, similar to CSCs (Paredez et al., 2006; Crowell et al., 2009; Gutierrez et al., 2009), the trafficking of GH9A1 occurs mainly between the Golgi apparatus, the *trans*-Golgi network, and the early endosomes.

### GH9A1 Interacts with Both Primary and Secondary CESAs

The association of GH9A1 and CSCs prompted us to test for direct interaction between CESA and GH9A1. Using in vitro affinity chromatography, interaction was detected for both the *Escherichia coli*–expressed, His-tagged, full-length GH9A1 and the His-tagged version of the predicted *jia1*-encoded GH9A1$^{A577V}$ with the *E. coli*–expressed, glutathione *S*-transferase (GST)–tagged central domains (CD) of two representative primary CESAs (GST-CESA1CD and GST-CESA3CD) and one secondary CESA (GST-CESA8CD) (Figures 4A and 4C). The amounts of His-tagged GH9A1 and His-tagged GH9A1$^{A577V}$ proteins bound by GST-CESACD proteins were similar, suggesting that the A577V amino acid substitution does not affect the binding of GH9A1 to CESAs.

### The *jia1* Mutation Abolishes the Endoglucanase Activity of GH9A1 in Vitro

*Arabidopsis* GH9A1 contains two glycosyl hydrolase family 9 active site signature motifs, with the signature 1 motif comprising residues Ser-499 to Arg-515 and the signature 2 motif comprising residues Tyr-559 to Ala-577 (Figure 4A; Supplemental Figure 2). The amino acid substitution (Ala-577 to Val) in *jia1-1* maps to the second signature motif of GH9A1. To test whether the amount of GH9A1$^{A577V}$ protein expressed in *jia1-1* is similar to GH9A1 expression levels in wild-type plants, total protein extracts from 10-d-old, light-grown seedlings were compared on immunoblots probed with anti-GH9A1 antiserum. The blots were also probed with an anti–α-tubulin monoclonal antibody as a loading control. The amount of GH9A1 protein detected in *jia1-1* extracts did not differ from that in wild-type plants (Figure 4B), indicating that the single A577V substitution affects a particular function of GH9A1 and that the phenotypes of *jia1-1* are not due to reduced levels of GH9A1.

To test whether the *jia1* mutation affects the endoglucanase activity of *Arabidopsis* GH9A1, wild-type GH9A1ΔN and GH9A1$^{A577V}$ΔN fragments (Figure 4A) were expressed in *Spodoptera frugiperda* Sf21 cells using a baculovirus expression system, which was recently shown to be suitable for the production of enzymatically active GH9A1 (Liebminger et al., 2013). Immunoblot analysis of cell extracts and culture supernatants revealed that recombinant wild-type GH9A1ΔN and the mutant GH9A1$^{A577V}$ΔN were successfully expressed in Sf21 cells and secreted into the culture medium. The secreted His6-tagged GH9A1ΔN and GH9A1$^{A577V}$ΔN proteins could be purified by means of nickel-chelate affinity chromatography in comparable yields. It was shown previously that CMC4M is a suitable substrate to assess the enzymatic activity of GH9A1 variants (Liebminger et al., 2013). Consistent with previous findings (Liebminger et al., 2013), wild-type GH9A1ΔN showed a specific activity of 317 ± 25 milliunits/mg with CMC4M. By contrast, the activity of GH9A1$^{A577V}$ΔN was barely detectable (4 ± 2 milliunits/mg; Figure 4D), suggesting that the *jia1* mutation abolishes the endoglucanase activity of *Arabidopsis* GH9A1.

### CSC Velocity Is Reduced in *jia1-1*

To monitor the dynamics of CSCs in *jia1-1* mutants, we introduced GFP-CESA3, a marker for CSCs (Desprez et al., 2007), into a homozygous *jia1-1* line. Although CSCs in the plasma membranes of *jia1-1* epidermal cells were organized into linear arrays as they are in wild-type seedlings, the velocity of CSCs was reduced in the mutant. In control cells, GFP-CESA3 had an average velocity of 312 ± 129 nm/min ($n$ = 882). In *jia1-1* mutants, however, the average velocity of GFP-CESA3 was reduced to 149 ± 72 nm/min ($n$ = 863; Figure 5A). This reduced velocity of GFP-CESA3 in *jia1-1* is evident in compiled kymographs as steeper CSC trace slopes from *jia1-1* images versus those of the wild type (Figure 5B). The reduced velocity is also reflected in the reduced mean frequency distribution of the velocities of GFP-CESA3 particles in *jia1-1* mutants, where more GFP-CESA3 particles were observed in *jia1-1* to have a velocity below 150 nm/min compared with those in control cells (Figure 5C). The reduction of CSC velocity in the *jia1-1* mutant suggests that GH9A1 influences the dynamics of CSCs, which reflects the reduced catalytic activities of *jia1-1* CSCs in vivo.

### Cellulose Microfibril Organization Is Altered in *jia1-1*

Atomic force microscopy (AFM) was used to examine the impact of defective GH9A1 on cellulose microfibril organization in the primary cell walls of *jia1-1* mutants. One prominent feature of the primary wall of *Arabidopsis* hypocotyls is that the cellulose microfibrils are arranged in multilayer sheets of varying angles (Figure 6A) (Chan et al., 2010). At the innermost wall surface, cellulose microfibrils appeared to have a nearly parallel alignment or to be bundled together, and multiple layers of cellulose microfibrils were not apparent in *jia1-1* plants (Figure 6A). In addition, cellulose microfibrils were less dispersed in *jia1-1* than those in the wild type, although the individual microfibril diameters were indistinguishable between the *jia1-1* mutant and the wild type (3.1 ± 0.2 nm). Cellulose microfibrils in wild-type cells displayed a wavy texture, which is similar to that observed in onion (*Allium cepa*) epidermis and cucumber (*Cucumis sativus*) hypocotyls (Marga et al., 2005; Zhang et al., 2013). By contrast, cellulose microfibrils of *jia1-1* had extensive abrupt kinks (45° ± 15°), which were rarely seen in the wild type (Figure 6B). Much larger kinks or discontinuations in cellulose microfibrils on the scale of micrometers were occasionally seen in onion epidermis that suffered mechanical damage during sample preparation (Supplemental Figure 5), leading us to speculate that the kinked cellulose microfibrils in *jia1-1* are likely not the result of mechanical damage during sample preparation. The abrupt kinks in *jia1-1* suggest a discontinuity of cellulose crystallinity, which may be induced by frequent disruptions during cellulose microfibril synthesis or aberrant microfibril mechanical strength.

To investigate the orientation and packing of cellulose microfibrils through the entire depth of the cell wall, vibrational sum frequency generation (SFG) spectroscopy was used. SFG can selectively detect the coherence of crystalline cellulose over several hundred nanometers within intact plant cell walls and thus is a nondestructive probe of the mesoscale ordering or packing of cellulose microfibrils (Barnette et al., 2011; Park

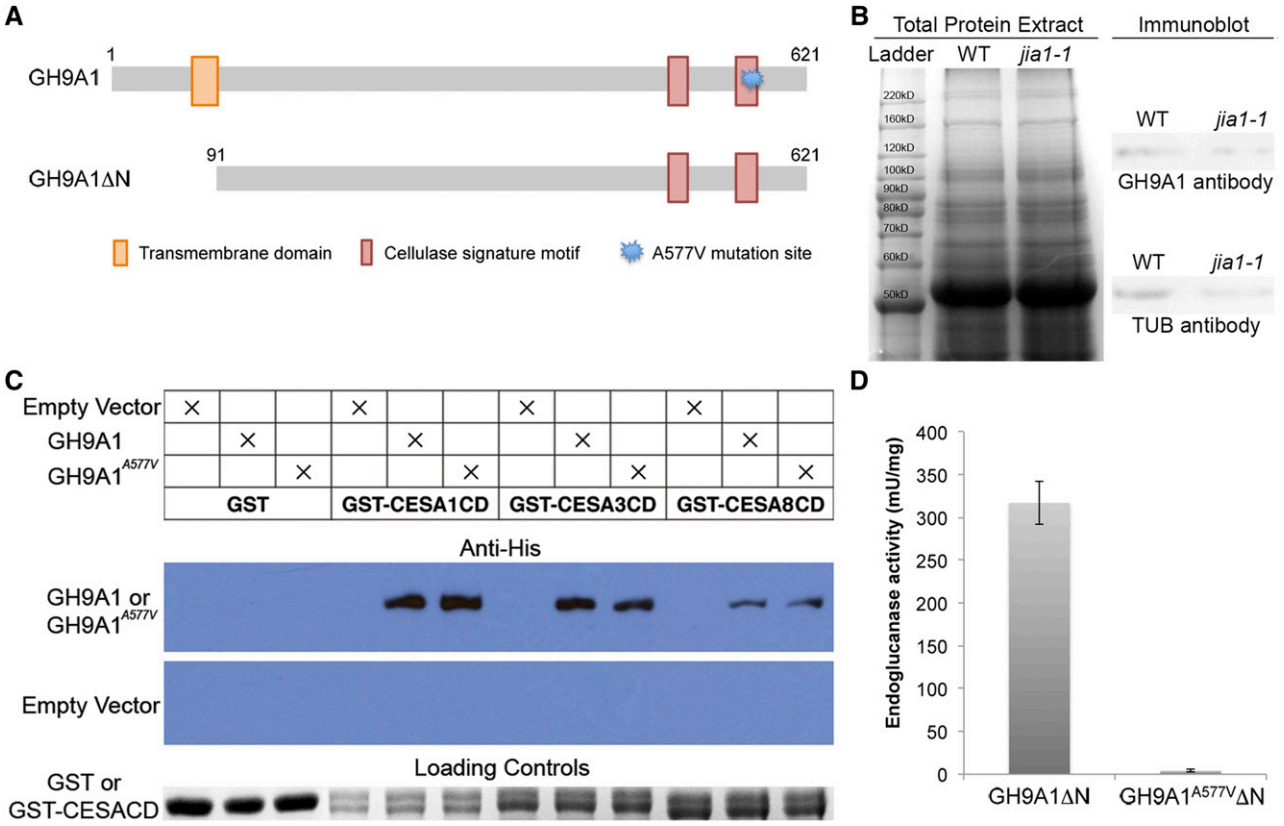


**Figure 4.** GH9A1$^{A577V}$ Abolishes the Endoglucanase Activity of GH9A1 but Not Its Interaction with CESAs.

**(A)** Schematic diagram of the GH9A1 protein structure.
**(B)** Immunoblot showing that the *jia1-1* mutation does not affect GH9A1 protein amount.
**(C)** GH9A1 and GH9A1$^{A577V}$ can interact with the central domains of CESA1, CESA3, and CESA8 in vitro. GST-CESA1CD, GST-CESA3CD, and GST-CESA8CD were used to bind His-tagged GH9A1 or His-tagged GH9A1$^{A577V}$ in vitro. Purified proteins from empty vector and GST alone were used as negative controls.
**(D)** Enzymatic activity of GH9A1ΔN and GH9A1$^{A577V}$ΔN using CMC4M as a substrate. Data are expressed as means ± SD of three experiments.
[See online article for color version of this figure.]

et al., 2013; Lee et al., 2014). The general features of the SFG peak shape of the wild-type and *jia1-1* spectra were similar to each other. Both showed a broad peak centered at 2920 cm$^{-1}$ in the alkyl (C-H and C-H$_2$) stretching region with a shoulder at 2968 cm$^{-1}$ and a strong peak centered at 3320 cm$^{-1}$ with a shoulder at 3450 cm$^{-1}$ in the hydroxyl (O-H) stretching region (Figures 6C and 6D). These are characteristics of primary cell walls and much different from cellulose microfibrils in secondary cell walls (Park et al., 2013; Kafle et al., 2014; Lee et al., 2014). Since the SFG intensity in the alkyl and hydroxyl regions varies depending on the orientation of the laser incidence plane and the orientation of cellulose alignment, the hydroxyl:alkyl ratio is one metric that can show the relative orientation of cellulose in the plant cell wall (Kafle et al., 2014). In SFG spectra of wild-type hypocotyls (Figure 6C), it is noticeable that the hydroxyl:alkyl SFG intensity ratio did not vary significantly ($P > 0.05$, Student's *t* test) when the sample was rotated with respect to the laser incidence plane. In SFG spectra of *jia1-1* hypocotyls (Figure 6D), the hydroxyl:alkyl ratio in the transverse direction (3.03 ± 0.56) was significantly higher than that in the longitudinal direction (1.68 ± 0.44). These results suggest that the cellulose microfibrils were preferentially arranged transverse to the long axis of the hypocotyl in *jia1-1* compared with the wild type. This is consistent with the AFM images of the innermost layer of cellulose microfibrils in *jia1-1*, which are more uniformly aligned than those in the wild type (Figures 6A and 6B). Since SFG is a nonlinear optical process, the intensity is sensitive not only to the cellulose amount in the probe volume but also to the pack density, orientation, and size of aggregated cellulose microfibrils within the coherence length, which is hundreds of nanometers to micrometers. Thus, the higher SFG intensity for the *jia1-1* mutant containing slightly less cellulose implies a better packing or ordering of cellulose microfibrils in the cell wall compared with the wild type (Supplemental Figure 6). Together, AFM and SFG spectra analysis suggest that the *jia1-1* mutant contains more transversely oriented cellulose microfibrils and better mesoscale packing or ordering than those in the wild type.

### Both CSC Tracks and Microtubule Organization Are Altered in *jia1-1*

To explore how microtubule organization might relate to changes in cellulose microfibril organization in *jia1-1*, we examined

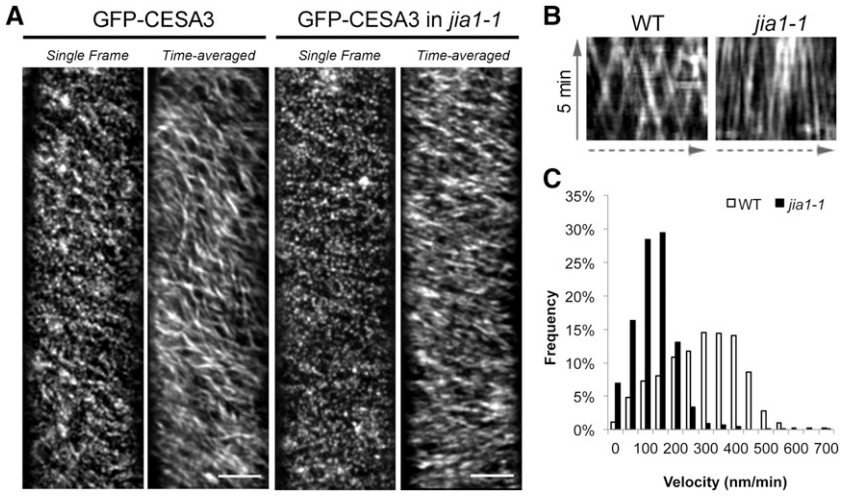


**Figure 5.** Loss of GH9A1 Results in Defective CSC Motility.

**(A)** Single optical sections and time averages of 61 frames (5-min duration in 5-s intervals) of GFP-CESA3 in the wild type and *jia1-1*. Bars = 5 μm.
**(B)** Kymographs of a linear GFP-CESA3 path in the wild type and *jia1-1*.
**(C)** Histogram of GFP-CESA3 particle velocities. The mean velocity is 312 ± 129 nm/min in the wild type ($n$ = 882) and 149 ± 72 nm/min in *jia1-1* ($n$ = 863).

microtubules in 3-d-old, dark-grown hypocotyl epidermal cells expressing GFP-MAP4 (Marc et al., 1998). The orientation of microtubules in epidermal cells showed spatial and temporal variation in *jia1-1* as compared with the wild type. To more easily describe the patterns we observed, the seedling hypocotyls were conceptually divided into three regions, upper (approximately six to eight cells), middle (approximately eight cells), and lower (approximately eight cells), termed zones 1, 2, and 3, respectively (Supplemental Figure 6A). Zone 1 is closer to the apical hook of dark-grown hypocotyls, and zone 1 cells are the most actively elongating of the three zones. Conversely, zone 3 is closer to the primary root, and most of the cells in this lower region have elongated completely. The orientation of epidermal cortical microtubules in zone 1 was mostly transverse, while that in zone 3 was longitudinal; zone 2 showed an oblique orientation of cortical microtubules, where a gradual transition from transverse to longitudinal was observed in both wild-type and *jia1-1* cells (Figure 7A; Supplemental Movie 5). In the wild type, ~7% of the cells observed had wavy, spaghetti-like microtubules in zone 1, as compared with ~23% in the same region of *jia1-1* (Figure 7B). These wavy microtubules were more frequently seen in *jia1-1* in zones 2 (~42%) and 3 (~62%). Fragmented microtubules were rarely observed in zones 1 and 2, and the frequency of fragmented microtubules in zone 3 was below 5% in wild-type hypocotyls. *jia1-1* had an increased frequency of fragmented microtubules in all zones, with the highest increases in zones 2 (13%) and 3 (18%). Collectively, these results indicate that microtubule organization is affected in the *jia1-1* mutant.

The trajectories of CSCs in the plasma membrane mirror the orientation of underlying cortical microtubules (Paredez et al., 2006; Crowell et al., 2009; Gutierrez et al., 2009; Li et al., 2012; Lei et al., 2013). To examine whether the *jia1* mutation affects the coalignment of CSCs and microtubules, *jia1-1* was crossed with a transgenic line expressing both GFP-CESA3 and mCherry-TUA5 (Gutierrez et al., 2009). The widespread coalignment between GFP-CESA3 and microtubules in *jia1-1* was evident, as highlighted by color tracks in two-channel confocal images (Figures 7C and 7D). In zone 3 *jia1-1* cells, where microtubule organization switched from transverse to longitudinal organization, the trajectory of an overlying GFP-CESA3 particle had a concomitant transverse-to-longitudinal reorientation (Figure 7D). Further supporting the coalignment between CSCs and microtubules, in *jia1-1* cells where disorganized microtubules were present, the trajectories of CSCs mirror the underlying disorganized microtubules (Supplemental Movie 6).

## DISCUSSION

*GH9A1* is an essential *Arabidopsis* gene whose conditional mutants show a collection of defects in several cellular functions, including cellulose synthesis in both primary and secondary cell walls, cytokinesis, microtubule organization, and hormonal responses (Nicol et al., 1998; Zuo et al., 2000; Szyjanowicz et al., 2004; Paredez et al., 2008). The proposed hypothetical cellulose proofreading, priming, and terminating functions of AtGH9A1 (Mølhøj et al., 2001a, 2002; Peng et al., 2002) are based on the presence of a luminal catalytic domain, which shares homology with a well-characterized bacterial EGase. While AtGH9A1 and its ortholog in *Brassica* have been reported to degrade amorphous cellulose in vitro, the precise role of GH9A1 is still unknown. Our study provided evidence that the endoglucanase activity of GH9A1 is important for proper cellulose biosynthesis in planta. The association of GH9A1 and CSCs is widespread in various intracellular compartments and at the plasma membrane, suggesting that GH9A1 might be an integral part of CSCs.

### Is the Endoglucanase Activity of GH9A1 Essential for Cellulose Synthesis in Plants?

*jia1*, encoding an A577V substitution in the second active site signature motif, is the only reported GH9A1 mutation that abolished

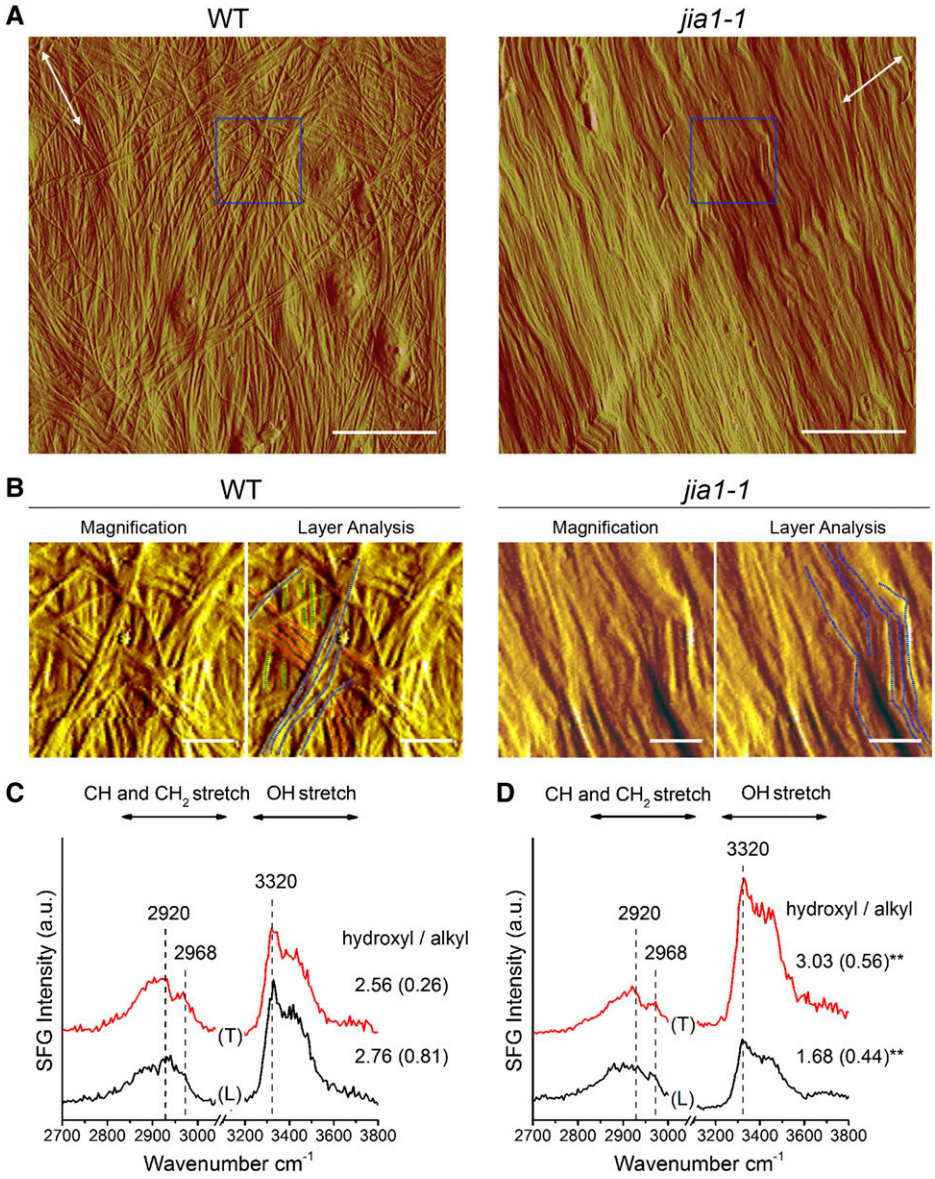


**Figure 6.** Cellulose Morphology Is Altered in *jia1-1*.

**(A)** AFM images of the inner cell wall of 3-d-old, dark-grown hypocotyls show different morphology of the cell wall for the wild type and *jia1-1*. Arrows indicate the long axis of the cells. Bars = 0.5 μm.

**(B)** Multiple layers of cellulose microfibrils were apparent in the wild type but not in *jia1-1*. Images are magnified from the highlighted squares in **(A)**. At least three layers of cellulose microfibrils were highlighted in green, red, and blue (innermost) dashed lines in wild-type samples. However, only one layer of cellulose microfibrils was observed in *jia1* samples, and these displayed multiple abrupt kinks highlighted by blue dashed lines. Bars = 0.1 μm.

**(C)** and **(D)** SFG spectra were taken from zone 1 (a region of hypocotyl close to the apical hook) of 4-d-old, dark-grown hypocotyls of the wild type **(C)** and *jia1-1* **(D)**. The samples were rotated so that the laser plane of incidence was along the long axis of the hypocotyl (L) and transverse to the long axis of the hypocotyl (T). The hydroxyl:alkyl ratios were calculated using the SFG intensities at 3320 and 2944 $cm^{-1}$ with the average and SD from $n = 4$ locations on the sample. Double asterisks indicate significant differences in hydroxyl:alkyl ratio ($P < 0.05$, Student's $t$ test). Spectra were normalized with respect to the peak at 2944 $cm^{-1}$. [See online article for color version of this figure.]

its endoglucanase activity in vitro. Considering the relatively mild phenotypes in both plant development and cellulose biosynthesis resulting from the *jia1* mutation, we propose that the endoglucanase activity of GH9A1 is an important, but nonessential, function for in vivo cellulose synthesis and plant viability. Although unlikely, we cannot exclude the possibility that the very low residual activity of $GH9A1^{A577V}$ is enough to sustain cellulose biosynthesis and plant viability, which might explain the difference between *kor1* null lethality and *jia1-1*. Alternatively, the physiological substrates for GH9A1 may not be

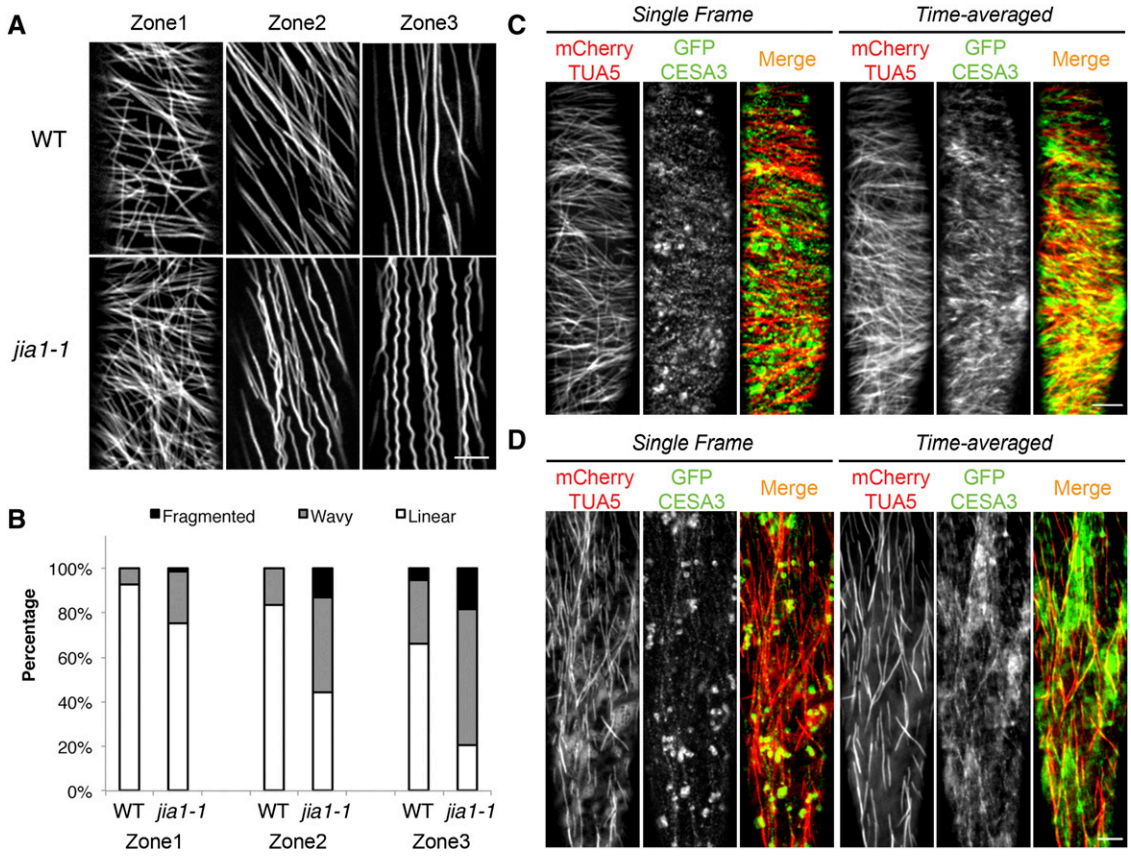


**Figure 7.** CSC Tracks and Microtubule Organization Are Altered in *jia1-1*.

Microtubules were visualized by confocal microscopy of GFP-MAP4 in epidermal cells of 3-d-old, dark-grown wild-type and *jia1-1* hypocotyls in **(A)** and **(B)**.

**(A)** *jia1-1* displays disorganized cortical microtubules, particularly in zones 2 and 3. Bar = 5 μm.

**(B)** Quantification of the microtubule organization pattern in the wild type and *jia1-1*. Data were collected from the measurement of ~400 cells from ~10 seedlings for each genotype.

**(C)** and **(D)** The coalignment between microtubules and CSCs is not affected in *jia1-1*. Single optical sections and time-averaged images of 61 frames (5-min duration in 5-s intervals) of dark-grown seedling epidermal cells expressing both mCherry-TUA5 and GFP-CESA3 show coalignment between CESA3 trajectories and cortical microtubules in zone 1 **(C)** and zone 3 **(D)**. Bars = 5 μm.

[See online article for color version of this figure.]

identical to those tested in vitro; thus, the GH9A1$^{A577V}$ mutant protein may yet be able to exhibit some degree of activity in vivo.

The importance of endoglucanases in bacterial cellulose synthesis has been firmly established. In *Gluconacetobacter xylinus*, an open reading frame is located upstream of the *bcs* operon, which encodes the EGase CMCax. CMCax is secreted by *G. xylinus*, and its endoglucanase activity is essential for cellulose synthesis in vivo but not in vitro (Standal et al., 1994; Kawano et al., 2002). While CMCax is a single gene in *G. xylinus*, *Arabidopsis* encodes two GH9A1-like genes: GH9A2 and GH9A3. It is possible that GH9A2 and/or GH9A3 can functionally compensate for the lack of endoglucanase activity in GH9A1$^{A577V}$, allowing the *jia1-1* mutant to retain cellulose synthesis ability yet not at full capacity. However, gene expression data show that GH9A2 and GH9A3 are expressed in specialized cells/tissues, such as root hairs, trichomes, and leaf vasculature (Mølhøj et al., 2001b). Therefore, it is unlikely that GH9A2 and/or GH9A3 can effectively substitute for GH9A1 and accommodate the cellulose biosynthetic requirements for the entire plant, taking into account that cellulose synthesized in specific cells is not transported intercellularly. Functional characterization of a double or triple mutant will be valuable to determine whether the combined endoglucanase activities of GH9A1 and GH9A1-like proteins are essential for cellulose synthesis in plants.

### KOR1 Is Associated with CSCs

A number of lines of evidence indicate that GH9A1 is important for cellulose biosynthesis, probably through a direct physical association between GH9A1 and CSCs (Nicol et al., 1998; His

et al., 2001; Lane et al., 2001; Mølhøj et al., 2001a, 2002; Sato et al., 2001; Szyjanowicz et al., 2004; Paredez et al., 2008). GFP-GH9A1 is not only colocalized with CSCs in the Golgi and *trans*-Golgi network but also in SmaCCs/MASCs, an intracellular compartment that has been implicated to be important for the delivery and/or recycling of CESAs (Crowell et al., 2009; Gutierrez et al., 2009). The colocalization of GFP-GH9A1 and mCherry-CESA3 is extensive at the plasma membrane. The average velocity of GFP-GH9A1 at the plasma membrane was ~340 nm/min, which is similar to what has been reported for CSCs and their associated proteins (Paredez et al., 2006; Desprez et al., 2007; Gu et al., 2010; Bischoff et al., 2011; Li et al., 2012). Further supporting a direct physical association between GH9A1 and CSCs, the *jia1* mutation resulted in an ~50% reduction of CSC velocity. The colocalization between GH9A1 and CSCs at multiple locations suggests that there might be a direct association between CSCs and GH9A1. Supporting this hypothesis, in vitro binding assays revealed the direct interaction between GH9A1 and multiple CESA proteins, including CESA1, CESA3, and CESA8.

### GH9A1 and Microtubule Organization

Mounting evidence supports the hypothesis that the orientation of newly synthesized cellulose microfibrils is determined by the underlying cortical microtubules (Green, 1962; Hepler and Newcomb, 1964; Baskin, 2001; Paredez et al., 2006). However, the mechanistic details of how microtubules control the organization of cellulose microfibrils remained unclear until the recent discovery of CELLULOSE SYNTHASE INTERACTIVE PROTEIN1 (CSI1), a linker between CSCs and microtubules (Gu et al., 2010; Gu and Somerville, 2010; Li et al., 2012). CSI1 is indispensable for the guidance of CSCs along cortical microtubules and is required to maintain the normal motility of CSCs. Similar to CSI1, GH9A1 colocalizes with CSCs and travels in a speed indistinguishable from that of CSCs. However, the coalignment between CSCs and cortical microtubules was not affected in the *jia1-1* mutant. Further supporting that GH9A1 is dispensable for the coalignment of CSCs and cortical microtubules, the CSC tracks mirrored the disorganized microtubules in *jia1-1*. CSI1 is required to maintain the normal velocity of CSCs, a function that may be microtubule dependent (Lei et al., 2012, 2014; Li et al., 2012, 2014). Similarly, the *jia1* mutation also reduced CSC velocity, a reduction that is more comparable to that of the *csi1 csi3* double mutant than that of *csi1* (Lei et al., 2013). We hypothesize that the reduction of CSC velocity in *jia1* is most likely not through CSI1/microtubule function, since the coalignment of CSCs and microtubules is normal in *jia1*. However, we cannot rule out the possibility that GH9A1 may assist the motility of CSCs at the membrane through a microtubule-dependent mechanism. Experiments to examine the CSC motility in the *jia1 csi1* double or *jia1 csi1 csi3* triple mutant are under way to test the above hypothesis.

The microtubule defect in *jia1* may be due to feedback regulation between the cell wall and the cytoskeleton (Wyatt and Carpita, 1993; Fisher and Cyr, 1998). Elimination of CSCs by either pharmacological or genetic means supports that dynamic reciprocity exists between the intracellular microtubules and the extracellular cell wall (DeBolt et al., 2007a, 2007b; Paredez et al., 2008). For example, 2,6-dichlorobenzonitrile, an inhibitor of cellulose synthesis, disrupted microtubule organization at a concentration of 0.5 μM (Peng et al., 2013). At a much higher concentration (5 μM), 2,6-dichlorobenzonitrile caused a complete loss of CSC motility at the plasma membrane (DeBolt et al., 2007b). Another drug, morlin (7-ethoxy-4-methyl chromen-2-one), is able to disrupt both microtubule organization and CSC motility (DeBolt et al., 2007a). *kor1-3* and a null allele of *CESA6* (*cesa6*$^{prc1\text{-}20}$) were identified in a screen for *Arabidopsis* mutants that are hypersensitive to oryzalin, a microtubule-depolymerizing drug, in which both mutants exhibited altered cortical microtubule orientation (Paredez et al., 2008). Interestingly, CSC motility is also reduced in *kor1-3* and *cesa6*$^{prc1\text{-}20}$. Together with the observations that cortical microtubule orientation was altered and CSC velocity was reduced in *jia1*, it is tempting to speculate that a reduced cellulose synthesis rate might be tightly associated with defects in microtubule organization. It is exciting that, in addition to CSI1, GH9A1 may represent a novel class of proteins involved in the intimate interaction between CSCs and microtubules. Further experiments are required to elucidate how the behavior of CSCs affects the underlying cortical microtubule organization.

### GH9A1 and Cellulose Microfibril Organization

Recently, AFM was developed to visualize nascent cellulose microfibrils at the inner surface of cell walls in onion epidermal cells. This method allows the visualization of cellulose microfibrils with minimal disturbance and in near-native conditions (Zhang et al., 2013). Applying this method, microfibrils in intact *Arabidopsis* tissues are revealed in unprecedented detail. Two interesting observations of cellulose microfibril organization were made in *jia1-1* mutant plants: abrupt kinks and loss of multilayer organization. Cellulose microfibrils often exist as bundles in both primary and secondary cell walls (Fernandes et al., 2011; Thomas et al., 2013; Zhang et al., 2013; Li et al., 2014). It is apparent that the kinks in *jia1-1* are at the same scale as cellulose microfibril bundles. Based on the prevalence and the size of the kinks observed in *jia1-1*, they are unlikely to be artifacts resulting from sample preparation. As such, kinks were also observed in the microtubules of the *jia1-1* mutant, so it is likely that the formation of kinks is attributable to defective microtubule organization. The defects in microtubule organization may result in disorganized secretion of noncellulosic cell wall materials such as hemicelluloses and pectins, which may result in an uneven coating of cellulose microfibrils by these materials, therefore influencing the local mechanical strength of cellulose microfibrils. Alternatively, the formation of these kinks may be independent of microtubule function. For example, kinks may be formed via the unsynchronized rate of individual elementary cellulose synthesis and the abrupt disruption of cellulose synthesis. Further research is needed to elucidate the exact mechanism for altered cellulose microfibril organization in *jia1-1*, possibly through a comparison of cellulose microfibril organization between *jia1-1* and various cellulose-deficient mutants.

As vibrational SFG spectroscopy can selectively detect the signal from crystalline cellulose within intact plant cell walls

(Barnette et al., 2011; Park et al., 2013), cellulose content, orientation, and mesoscale ordering of cellulose microfibrils can be reflected in the intensity and hydroxyl:alkyl ratio of SFG spectra. *jia1-1* shows a reduced crystalline cellulose content as determined by the Updegraff method (Updegraff, 1969). However, the SFG intensity was slightly stronger in *jia1-1* than in the wild type. The apparent discrepancy can be attributed to the compensation of the signal from the increased ordering of cellulose microfibrils as compared with that in the wild type. The altered intensity and the hydroxyl:alkyl ratio of *jia1-1* SFG spectra suggested that the cellulose microfibrils in *jia1-1* had more mesoscale lateral packing. This raises the question of why *jia1-1* mutants had more transversely oriented cellulose microfibrils but reduced cell elongation. It is known that the cellulose microfibrils are oriented transversely in the innermost plant epidermal cell walls, thus favoring longitudinal expansion (Roelofsen and Houwink, 1951; Roelofsen et al., 1953). However, during cell elongation, layers of cellulose microfibrils rotate as sheets of varying angles, which establish the basis of the multinet growth hypothesis (Green, 1960; Roelofsen, 1965; Roland et al., 1975). It has been hypothesized that multinet cellulose organization may relate to the features of the primary cell walls, such as extensibility and rigidity (Li et al., 2014). It is likely that the loss of multinet cellulose organization in *jia1-1* may affect the mechanical strength of the cell wall. It is also possible that the localized incorporation of other wall polymers might be affected in *jia1*, thus affecting the overall mechanical strength of cell wall. Reduced overall crystalline cellulose content in hypocotyls and abrupt kinks in *jia1-1* mutants support the idea that the mechanical strength of the cell wall might be affected.

Consistent with the multinet hypothesis, the underlying cortical microtubules as well as CSC trajectories undergo relative rotary movements in the successive layers of cellulose in *Arabidopsis* hypocotyl epidermal cells (Chan et al., 2007; Zhang et al., 2013; Bashline et al., 2014). Pharmacological disruption of microtubule rotation inhibited the rotation of CSC trajectories, leading to the hypothesis that the rotation of cellulose microfibrils is dependent on microtubule organization (Chan et al., 2007, 2010, 2011; Chan, 2012). The loss of multiple-angle layers of cellulose microfibrils in *jia1-1* may be attributed to the defect in microtubule organization. However, the coalignment of microtubules and cellulose microfibrils was not affected in *jia1-1*. Alternatively, the *jia1* mutation might induce hormonal response defects, thus affecting cell elongation. One severe mutant of *GH9A1*, *tsd1*, was reported to have defects in response to auxin and cytokinin, two hormones that are involved in coordinating plant growth (Krupková and Schmülling, 2009). Other factors, such as biophysical forces and turgor-driven expansion, may also influence cellulose microfibril reorientation. Further characterization of *jia1* will shed light on the mechanism(s) underlying microtubule organization and cell wall architecture in plants.

## METHODS

### Transgenic Lines

The 35S promoter in pGWB2 was replaced with a 2-kb CESA3 promoter using *Hin*dII and *Xba*I to create the construct pYG114 using the primers indicated in Supplemental Table 1. The full-length coding sequences of CESA3 and mCherry were amplified using the primers indicated in Supplemental Table 1, ligated together at an introduced *Xba*I site, and cloned into the pCR8/GW/TOPO vector (Life Technologies) to create the construct pYG115. The sequence-verified mCherry-CESA3 fragment was cloned into the pGWB2 vector that contained the native *CESA3* promoter using Gateway LR Clonase II (Life Technologies) to produce pYG116. pYG116 was transformed into *je5* by *Agrobacterium tumefaciens*–mediated transformation. mCherry-CESA3 transgenic lines selected for further analysis were designated YG108 and YG109. To generate GFP-GH9A1 transgenic lines, the 35S promoter in pH7FWG2 (Karimi et al., 2002) was replaced by a 2-kb *GH9A1* promoter using the primers indicated in Supplemental Table 1 to create pYG117. The full-length coding sequence of *GH9A1* was introduced into pYG118 using Gateway LR Clonase II. The sequence-verified construct pYG119 was introduced into *kor1-3* using *Agrobacterium*-mediated transformation. GFP-GH9A1 transgenic lines selected for further analysis were designated YG110 and YG111. An mCherry-CESA3–expressing *Arabidopsis thaliana* line was crossed with one expressing GFP-GH9A1 to create the double-labeled transgenic lines.

### Protein Purification and in Vitro Binding/Affinity Chromatography Assay

The coding sequences of the central domains of *CESA1*, *CESA3*, and *CESA8* were cloned into the pGEX-KG vector in frame with an N-terminal GST tag and expressed in BL21Star-pLysS *Escherichia coli*. The *GH9A1* wild-type coding sequence and *GH9A1*$^{A577V}$ coding sequence were cloned into YG201, which provides an N-terminal His tag protein fusion, and expressed in BL21-CodonPlus (DE3)-RIPL *E. coli*. Protein was induced with 1 mM isopropyl β-D-1-thiogalactopyranoside at 15°C for 20 h. Protein purification and an in vitro pull-down assay were performed as described previously (Bashline et al., 2013).

### Immunoblot Analysis

Proteins were separated by SDS-PAGE and transferred to nitrocellulose membranes. Immunostaining was performed by blocking the nitrocellulose membrane with PBS and 0.1% Tween 20 (PBS-T) containing 5% nonfat milk followed by incubation for 2 h at room temperature with the anti-AtGH9A1 antiserum diluted 1:2000 or anti–α-tubulin monoclonal antibody, clone B-5-1-2 (Sigma-Aldrich), diluted 1:8000 in PBS-T. After extensive washing with PBS-T, membranes were incubated for 2 h at room temperature with goat anti-rabbit or goat anti-mouse antibodies conjugated to peroxidase (Santa Cruz) diluted 1:10,000 in PBS-T containing 5% milk. Detection of antibody binding was performed using the ECL-Select protein gel blotting reagent and the ImageQuant LAS 4000 digital imaging system (GE Healthcare Life Sciences).

### Site-Directed Mutagenesis of GH9A1

The GH9A1$^{A577V}$-encoding construct was generated using the QuikChange Site-Directed Mutagenesis Kit (Stratagene) and Phusion High-Fidelity DNA Polymerase (Life Technologies). Mutagenesis was performed following the manufacturer's instructions. The wild-type pVTBacHis-GH9A1 construct (Liebminger et al., 2013) was used as a template for site-directed mutagenesis using the primers indicated in Supplemental Table 1. To confirm the introduced mutations, all constructs were subjected to DNA sequencing.

### Expression of GH9A1 Variants in Insect Cells and GH9A1 Activity Assays

Cultivation of *Spodoptera frugiperda* Sf21 cells, baculovirus-mediated infection, and purification of the recombinant proteins were performed as described in detail previously (Liebminger et al., 2013). At the end of the purification procedure, the GH9A1-containing fractions were pooled and concentrated by ultrafiltration and then subjected to diafiltration using assay buffer containing 50 mM MES, pH 6.0, 250 mM NaCl, and 30 mM $CaCl_2$.

Purified recombinant GH9A1 (0.3 to 1 μg, 10 μL) was incubated with 90 μL of 0.1% CMC4M (Megazyme) in assay buffer for 90 min at 30°C. The reaction was stopped by the addition of 400 μL of ice-cold 50 mM sodium borate, pH 10.0. Then, 500 μL of freshly prepared BCA solution (a mixture of equal volumes of reagent A containing 5 mM 2,2′-bicinchoninic acid, 512 mM $Na_2CO_3$, and 288 mM $NaHCO_3$ and reagent B containing 5 mM $CuSO_4$ and 12 mM L-Ser) was added, and the samples were incubated for 15 min at 95°C. The samples were cooled on ice and then centrifuged for 3 min prior to measurement of their absorbance at 562 nm. Samples containing heat-inactivated enzyme were used as controls. The amount of reducing ends generated was then deduced using a Glc standard curve (0 to 25 nmol). All assays were done in duplicate.

### Live-Cell Imaging

Dark-grown hypocotyls were grown on vertical MS plates [half-strength MS salts, 0.8% agar, and 0.05% 2-(*N*-morpholino)ethanesulfonic acid monohydrate, pH 5.7] in the dark at 22°C for 3 d. Images were obtained of epidermal cells within 2 mm of the apical hook unless indicated otherwise. Imaging was performed on a Yokogawa CSUX1 spinning-disk system as described previously (Gu et al., 2010; Bashline et al., 2014). Image analysis was performed using Metamorph (Molecular Devices), ImageJ, and Imaris (Bitplane) software. CESA particle dynamics analyses were performed as described previously (Gu et al., 2010; Bashline et al., 2014).

### AFM of *Arabidopsis* Hypocotyl Walls

Hypocotyls of wild-type *Arabidopsis* (Col-0) and *jia1* mutants were grown in the dark as described above for 3 d before being collected and stored at −80°C for less than 1 week. Hypocotyls were ground in liquid nitrogen and rinsed with 20 mM HEPES buffer, pH 7.0, and 0.1% Tween 20 until the filtrate was clear. One droplet of well-resuspended hypocotyl walls was added onto a clean glass slide, and excess buffer was evaporated but the sample still remained visibly moist (~5 min). To remove any loosely bound cell wall fragments, the wall samples were rinsed and rehydrated with 20 mM HEPES before scanning. *Arabidopsis* hypocotyl epidermis was scanned by an atomic force microscope (Bruker; Dimension Icon). A light microscope was used to identify the unique rectangular shape of epidermal cell wall fragments from the hypocotyls. Throughout scanning, the samples were submerged in 20 mM HEPES, pH 7.0. ScanAsyst and PeakForce Tapping mode were used to operate the AFM. SCANASYST-FLUID+ probes (Bruker) with a spring constant of between 0.2 and 0.7 N/m were chosen for all experiments. All images (scan size of 2 μm) were scanned at a 512 × 512 sampling rate. At least five different cells or fragments from each sample were scanned, and representative images were chosen for analysis.

### SFG Spectroscopy of *Arabidopsis* Hypocotyl Walls

In SFG, two high-intensity laser pulses with visible ($\omega_{VIS}$) and infrared ($\omega_{IR}$) frequencies are overlapped on the sample. When the frequency of the infrared photon resonates with the noncentrosymmetrically arranged vibration modes, a third SFG photon is generated as the sum of the two input photons ($\omega_{SFG} = \omega_{VIS} + \omega_{IR}$). In plant cell walls, only the vibration modes within the bulk cellulose crystals are arranged noncentrosymmetrically and thus are SFG active; the matrix polymers are randomly arranged and therefore cannot generate SFG. The SFG intensity is sensitive to the arrangement of cellulose microfibrils over the optical coherence length, which is 290 to 310 nm (Lee et al., 2014).

Hypocotyls of wild-type *Arabidopsis* (Col-0) and *jia1* mutants were grown in the dark as described above for 4 d before being collected and stored at −80°C for less than 1 week. After defrosting and rinsing with distilled, deionized water, 20 to 30 hypocotyls were closely aligned side-by-side on a glass slide and air-dried for 3 d. The SFG spectroscopic measurements were performed in reflection geometry, irradiating the sample with picosecond laser pulses of p-polarized infrared and s-polarized visible wavelengths and detecting the emitted SFG signals, which were not polarized. The details of SFG measurements were published previously (Barnette et al., 2011). The SFG spectrometer (EKSPLA) was pumped by a picosecond Nd:YAG laser, 1064 nm at 10 Hz. An optical parameter generator/amplifier was pumped with 532 and 1064 nm and tuned to 2.3 to 10 μm with <6 $cm^{-1}$ bandwidth. Visible (60° to surface normal) and infrared (56°) laser pulses were overlapped spatially and temporally on each sample with reflection geometry. A beam collimator was used to enhance the signal collection efficiency, and the SFG signal was filtered through a monochromator and detected with a photomultiplier tube (Hamamatsu). The SFG intensity was normalized with incident infrared and visible laser intensities. SFG spectra were taken at 4 $cm^{-1}$/step in the C-H and C-$H_2$ stretching region (2700 to 3050 $cm^{-1}$) and at 8 $cm^{-1}$/step in the O-H stretching region (3096 to 3800 $cm^{-1}$). The probe volume was estimated to be ~150 × 200 $\mu m^2$ wide and ~20 μm deep from the external surface, which is governed by the infrared beam attenuation in the sample (Kafle et al., 2014).

Depending on the location on the sample, there was some variability in the absolute SFG intensity. To address the variation in texture and stacking of multiple hypocotyls during the drying process, the average SFG intensities at 2944 and 3320 $cm^{-1}$ were first taken from four locations on the samples. The complete SFG spectra were taken at locations on the sample where the SFG signal was equal to the average intensity obtained from these four locations. The hydroxyl/alkyl values were taken from the intensities at 2944 and 3320 $cm^{-1}$ from the four chosen locations. Each SFG spectrum was taken with the laser plane of incidence parallel to (Figures 6C and 6D, black curve) or transverse to (Figures 6C and 6D, red curve) the hypocotyl axis. Each spectrum was normalized over the intensity at 2944 $cm^{-1}$ to visualize the changes in the SFG intensity in the OH stretching region (3096 to 3800 $cm^{-1}$).

### Cellulose Content Measurements

Crystalline cellulose was measured in 4-d-old, dark-grown seedlings using the Updegraff method (Updegraff, 1969). Data were collected from five technical replicates for each tissue sample.

### Accession Numbers

Sequence data from this article can be found in the Arabidopsis Genome Initiative or GenBank/EMBL databases under the following accession numbers: *Arabidopsis thaliana* GH9A1 (AtGH9A1), AT5G49720; *Vitis vinifera* GH9A1 (VvGH9A1), GSVIVG01006265001; *Ricinus communis* GH9A1 (RcGH9A1), 30,063.t000040; *Populus trichocarpa* GH9A1 (PtGH9A1), Potri.010G177300; *Oryza sativa* GH9A1 (OsGH9A1), LOC_Os04g41970; *Brachypodium distachyon* GH9A1 (BdGH9A1), Bradi1g63560; *Setaria italica* GH9A1 (SiGH9A1), Si034713m; *Sorghum bicolor* GH9A1 (SbGH9A1), Sb01g008860; *Selaginella moellendorffii* GH9A1 (SmGH9A1), 266522; *Physcomitrella patens* GH9A1 (PpGH9A1), Pp1s64_152V6; and *Chlamydomonas reinhardtii* GH9A1 (CrGH9A1), Cre06.g270500.

### Supplemental Data

The following materials are available in the online version of this article.

**Supplemental Figure 1.** *jia1-1* Is Allelic to *kor1-3*.

**Supplemental Figure 2.** Homology between the Amino Acid Sequences of GH9A1 Shows That Ala-577 Is Highly Conserved.

**Supplemental Figure 3.** Morphology of *jia1-1*.

**Supplemental Figure 4.** GH9A1 Is Located in Various Intracellular Organelles.

**Supplemental Figure 5.** AFM Images Show Mechanical Damage during Sample Preparation.

**Supplemental Figure 6.** SFG Spectra of 4-d-Old Dark-Grown Hypocotyls of the Wild Type and *jia1-1*.

**Supplemental Table 1.** DNA Primers Used in This Study.

**Supplemental Movie 1.** GH9A1 Localizes to Distinct Particles at the Plasma Membrane.

**Supplemental Movie 2.** Dynamic Association between GH9A1 and CESA Complexes at the Plasma Membrane.

**Supplemental Movie 3.** Dynamic Association between GH9A1 and CESA Complexes in Intracellular Compartments.

**Supplemental Movie 4.** Dynamic Association between GH9A1 and SYP32 in the Golgi Apparatus and the *trans*-Golgi Network.

**Supplemental Movie 5.** Microtubule Organization in the Wild Type and *jia1-1*.

**Supplemental Movie 6.** Disorganized Microtubule Bundles Coalign with Disorganized CSC Tracks in the *jia1-1* Mutant.

### ACKNOWLEDGMENTS

We thank Barbara Svoboda for technical assistance with GH9A1 activity assays. We thank Ryan Gutierrez and David Ehrhardt for providing the mCherry-TUA5 GV3101 strain. We thank Herman Höfte for providing GFP-CESA3 transgenic seeds. We thank Niko Geldner for providing mCherry-SYP32, -SYP61, -VIT12, -RabC1, -RabA1g, and -RabG3f transgenic seeds. We thank Yong Bum Park for technical assistance on sample preparation for SFG analysis. We thank Colleen McMichael for critical reading of the article. This work was supported by the Center for LignoCellulose Structure and Formation, an Energy Frontier Research Center funded by the U.S. Department of Energy, Office of Science, Office of Basic Sciences (Grant DE-SC0001090), and by the National Science Foundation (Grant 1121375 for mCherry-CESA and GFP-KOR1 transgenic line production and CESA central domain expression).

### AUTHOR CONTRIBUTIONS

S.L. and Y.G. designed research. L.L., S.L., T.Z., R.S., C.M.L., and M.G. performed research. T.Z. and D.J.C. conducted atomic force microscopy analysis of *jia1*. R.S. and L.M. performed GH9A1 activity assays. C.M.L. and S.H.K. performed SFG analysis of *jia1*. M.G. and S.V. conducted immunoblot analysis of *jia1*. L.L. and S.L. performed the rest of the experiments. L.L., S.L., T.Z., R.S., C.M.L., S.H.K., D.J.C., and Y.G. analyzed data. S.L., L.L., T.Z., R.S., C.M.L., and Y.G. wrote the article.

Received April 4, 2014; revised May 30, 2014; accepted June 10, 2014; published June 24, 2014.

### REFERENCES

**Barnette, A.L., Bradley, L.C., Veres, B.D., Schreiner, E.P., Park, Y.B., Park, J., Park, S., and Kim, S.H.** (2011). Selective detection of crystalline cellulose in plant cell walls with sum-frequency-generation (SFG) vibration spectroscopy. Biomacromolecules **12:** 2434–2439.

**Bashline, L., Lei, L., Li, S., and Gu, Y.** (2014). Cell wall, cytoskeleton, and cell expansion in higher plants. Mol. Plant **7:** 586–600.

**Bashline, L., Li, S., Anderson, C.T., Lei, L., and Gu, Y.** (2013). The endocytosis of cellulose synthase in Arabidopsis is dependent on μ2, a clathrin-mediated endocytosis adaptin. Plant Physiol. **163:** 150–160.

**Baskin, T.I.** (2001). On the alignment of cellulose microfibrils by cortical microtubules: A review and a model. Protoplasma **215:** 150–171.

**Bischoff, V., Desprez, T., Mouille, G., Vernhettes, S., Gonneau, M., and Höfte, H.** (2011). Phytochrome regulation of cellulose synthesis in Arabidopsis. Curr. Biol. **21:** 1822–1827.

**Brummell, D.A., Catala, C., Lashbrook, C.C., and Bennett, A.B.** (1997). A membrane-anchored E-type endo-1,4-beta-glucanase is localized on Golgi and plasma membranes of higher plants. Proc. Natl. Acad. Sci. USA **94:** 4794–4799.

**Chan, J.** (2012). Microtubule and cellulose microfibril orientation during plant cell and organ growth. J. Microsc. **247:** 23–32.

**Chan, J., Calder, G., Fox, S., and Lloyd, C.** (2007). Cortical microtubule arrays undergo rotary movements in Arabidopsis hypocotyl epidermal cells. Nat. Cell Biol. **9:** 171–175.

**Chan, J., Crowell, E., Eder, M., Calder, G., Bunnewell, S., Findlay, K., Vernhettes, S., Höfte, H., and Lloyd, C.** (2010). The rotation of cellulose synthase trajectories is microtubule dependent and influences the texture of epidermal cell walls in Arabidopsis hypocotyls. J. Cell Sci. **123:** 3490–3495.

**Chan, J., Eder, M., Crowell, E.F., Hampson, J., Calder, G., and Lloyd, C.** (2011). Microtubules and CESA tracks at the inner epidermal wall align independently of those on the outer wall of light-grown Arabidopsis hypocotyls. J. Cell Sci. **124:** 1088–1094.

**Crowell, E.F., Bischoff, V., Desprez, T., Rolland, A., Stierhof, Y.D., Schumacher, K., Gonneau, M., Höfte, H., and Vernhettes, S.** (2009). Pausing of Golgi bodies on microtubules regulates secretion of cellulose synthase complexes in *Arabidopsis*. Plant Cell **21:** 1141–1154.

**Crowell, E.F., Gonneau, M., Stierhof, Y.D., Höfte, H., and Vernhettes, S.** (2010). Regulated trafficking of cellulose synthases. Curr. Opin. Plant Biol. **13:** 700–705.

**DeBolt, S., Gutierrez, R., Ehrhardt, D.W., Melo, C.V., Ross, L., Cutler, S.R., Somerville, C., and Bonetta, D.** (2007a). Morlin, an inhibitor of cortical microtubule dynamics and cellulose synthase movement. Proc. Natl. Acad. Sci. USA **104:** 5854–5859.

**DeBolt, S., Gutierrez, R., Ehrhardt, D.W., and Somerville, C.** (2007b). Nonmotile cellulose synthase subunits repeatedly accumulate within localized regions at the plasma membrane in Arabidopsis hypocotyl cells following 2,6-dichlorobenzonitrile treatment. Plant Physiol. **145:** 334–338.

**Desprez, T., Juraniec, M., Crowell, E.F., Jouy, H., Pochylova, Z., Parcy, F., Höfte, H., Gonneau, M., and Vernhettes, S.** (2007). Organization of cellulose synthase complexes involved in primary cell wall synthesis in *Arabidopsis thaliana*. Proc. Natl. Acad. Sci. USA **104:** 15572–15577.

**Desprez, T., Vernhettes, S., Fagard, M., Refrégier, G., Desnos, T., Aletti, E., Py, N., Pelletier, S., and Höfte, H.** (2002). Resistance against herbicide isoxaben and cellulose deficiency caused by distinct mutations in same cellulose synthase isoform CESA6. Plant Physiol. **128:** 482–490.

**Fernandes, A.N., Thomas, L.H., Altaner, C.M., Callow, P., Forsyth, V.T., Apperley, D.C., Kennedy, C.J., and Jarvis, M.C.** (2011).

Nanostructure of cellulose microfibrils in spruce wood. Proc. Natl. Acad. Sci. USA **108:** E1195–E1203.

**Fisher, D.D., and Cyr, R.J.** (1998). Extending the microtubule/microfibril paradigm: Cellulose synthesis is required for normal cortical microtubule alignment in elongating cells. Plant Physiol. **116:** 1043–1051.

**Geldner, N., Dénervaud-Tendon, V., Hyman, D.L., Mayer, U., Stierhof, Y.D., and Chory, J.** (2009). Rapid, combinatorial analysis of membrane compartments in intact plants with a multicolor marker set. Plant J. **59:** 169–178.

**Green, P.B.** (1960). Multinet growth in the cell wall of Nitella. J. Biophys. Biochem. Cytol. **7:** 289–296.

**Green, P.B.** (1962). Mechanism for plant cellular morphogenesis. Science **138:** 1404–1405.

**Gu, Y., and Somerville, C.** (2010). Cellulose synthase interacting protein: A new factor in cellulose synthesis. Plant Signal. Behav. **5:** 1571–1574.

**Gu, Y., Kaplinsky, N., Bringmann, M., Cobb, A., Carroll, A., Sampathkumar, A., Baskin, T.I., Persson, S., and Somerville, C.R.** (2010). Identification of a cellulose synthase-associated protein required for cellulose biosynthesis. Proc. Natl. Acad. Sci. USA **107:** 12866–12871.

**Gutierrez, R., Lindeboom, J.J., Paredez, A.R., Emons, A.M., and Ehrhardt, D.W.** (2009). Arabidopsis cortical microtubules position cellulose synthase delivery to the plasma membrane and interact with cellulose synthase trafficking compartments. Nat. Cell Biol. **11:** 797–806.

**Haigler, C.H., and Brown, R.M.** (1986). Transport of rosettes from the Golgi apparatus to the plasma membrane in isolated mesophyll cells of *Zinnia elegans* during differentiation to tracheary elements in suspension culture. Protoplasma **134:** 111–120.

**Hepler, P.K., and Newcomb, E.H.** (1964). Microtubules and fibrils in the cytoplasm of coleus cells undergoing secondary wall deposition. J. Cell Biol. **20:** 529–532.

**His, I., Driouich, A., Nicol, F., Jauneau, A., and Höfte, H.** (2001). Altered pectin composition in primary cell walls of korrigan, a dwarf mutant of Arabidopsis deficient in a membrane-bound endo-1,4-beta-glucanase. Planta **212:** 348–358.

**Kafle, K., Xi, X., Lee, C.M., Tittmann, B., Cosgrove, D.J., Park, Y.B., and Kim, S.H.** (2014). Cellulose microfibril orientation in onion (*Allium cepa* L.) epidermis studied by atomic force microscopy (AFM) and vibrational sum frequency generation (SFG) spectroscopy. Cellulose **21:** 1075–1086.

**Karimi, M., Inzé, D., and Depicker, A.** (2002). GATEWAY vectors for Agrobacterium-mediated plant transformation. Trends Plant Sci. **7:** 193–195.

**Kawano, S., Tajima, K., Kono, H., Erata, T., Munekata, M., and Takai, M.** (2002). Effects of endogenous endo-beta-1,4-glucanase on cellulose biosynthesis in Acetobacter xylinum ATCC23769. J. Biosci. Bioeng. **94:** 275–281.

**Krupková, E., and Schmülling, T.** (2009). Developmental consequences of the tumorous shoot development1 mutation, a novel allele of the cellulose-synthesizing KORRIGAN1 gene. Plant Mol. Biol. **71:** 641–655.

**Lane, D.R., et al**. (2001). Temperature-sensitive alleles of RSW2 link the KORRIGAN endo-1,4-beta-glucanase to cellulose synthesis and cytokinesis in Arabidopsis. Plant Physiol. **126:** 278–288.

**Lee, C.M., Kafle, K., Park, Y.B., and Kim, S.H.** (2014). Probing crystal structure and mesoscale assembly of cellulose microfibrils in plant cell walls, tunicate tests, and bacterial films using vibrational sum frequency generation (SFG) spectroscopy. Phys. Chem. Chem. Phys. **16:** 10844–10853.

**Lei, L., Li, S., Bashline, L., and Gu, Y.** (2014). Dissecting the molecular mechanism underlying the intimate relationship between cellulose microfibrils and cortical microtubules. Front. Plant Sci. **5:** 90.

**Lei, L., Li, S., Du, J., Bashline, L., and Gu, Y.** (2013). Cellulose synthase INTERACTIVE3 regulates cellulose biosynthesis in both a microtubule-dependent and microtubule-independent manner in *Arabidopsis*. Plant Cell **25:** 4912–4923.

**Lei, L., Li, S., and Gu, Y.** (2012). Cellulose synthase interactive protein 1 (CSI1) mediates the intimate relationship between cellulose microfibrils and cortical microtubules. Plant Signal. Behav. **7:** 714–718.

**Li, S., Bashline, L., Lei, L., and Gu, Y.** (2014). Cellulose synthesis and its regulation. The Arabidopsis Book **12:** e0169, doi/10.1199/tab.0169.

**Li, S., Lei, L., Somerville, C.R., and Gu, Y.** (2012). Cellulose synthase interactive protein 1 (CSI1) links microtubules and cellulose synthase complexes. Proc. Natl. Acad. Sci. USA **109:** 185–190.

**Liebminger, E., Grass, J., Altmann, F., Mach, L., and Strasser, R.** (2013). Characterizing the link between glycosylation state and enzymatic activity of the endo-β1,4-glucanase KORRIGAN1 from *Arabidopsis thaliana*. J. Biol. Chem. **288:** 22270–22280.

**Marc, J., Granger, C.L., Brincat, J., Fisher, D.D., Kao, T., McCubbin, A.G., and Cyr, R.J.** (1998). A GFP-MAP4 reporter gene for visualizing cortical microtubule rearrangements in living epidermal cells. Plant Cell **10:** 1927–1940.

**Marga, F., Grandbois, M., Cosgrove, D.J., and Baskin, T.I.** (2005). Cell wall extension results in the coordinate separation of parallel microfibrils: Evidence from scanning electron microscopy and atomic force microscopy. Plant J. **43:** 181–190.

**Master, E.R., Rudsander, U.J., Zhou, W., Henriksson, H., Divne, C., Denman, S., Wilson, D.B., and Teeri, T.T.** (2004). Recombinant expression and enzymatic characterization of PttCel9A, a KOR homologue from *Populus tremula* × *tremuloides*. Biochemistry **43:** 10080–10089.

**Mølhøj, M., Johansen, B., Ulvskov, P., and Borkhardt, B.** (2001a). Expression of a membrane-anchored endo-1,4-beta-glucanase from *Brassica napus*, orthologous to KOR from *Arabidopsis thaliana*, is inversely correlated to elongation in light-grown plants. Plant Mol. Biol. **45:** 93–105.

**Mølhøj, M., Jørgensen, B., Ulvskov, P., and Borkhardt, B.** (2001b). Two *Arabidopsis thaliana* genes, KOR2 and KOR3, which encode membrane-anchored endo-1,4-beta-D-glucanases, are differentially expressed in developing leaf trichomes and their support cells. Plant Mol. Biol. **46:** 263–275.

**Mølhøj, M., Pagant, S., and Höfte, H.** (2002). Towards understanding the role of membrane-bound endo-beta-1,4-glucanases in cellulose biosynthesis. Plant Cell Physiol. **43:** 1399–1406.

**Nicol, F., His, I., Jauneau, A., Vernhettes, S., Canut, H., and Höfte, H.** (1998). A plasma membrane-bound putative endo-1,4-beta-D-glucanase is required for normal wall assembly and cell elongation in Arabidopsis. EMBO J. **17:** 5563–5576.

**Paredez, A.R., Persson, S., Ehrhardt, D.W., and Somerville, C.R.** (2008). Genetic evidence that cellulose synthase activity influences microtubule cortical array organization. Plant Physiol. **147:** 1723–1734.

**Paredez, A.R., Somerville, C.R., and Ehrhardt, D.W.** (2006). Visualization of cellulose synthase demonstrates functional association with microtubules. Science **312:** 1491–1495.

**Park, Y.B., Lee, C.M., Koo, B.W., Park, S., Cosgrove, D.J., and Kim, S.H.** (2013). Monitoring meso-scale ordering of cellulose in intact plant cell walls using sum frequency generation spectroscopy. Plant Physiol. **163:** 907–913.

**Peng, L., Kawagoe, Y., Hogan, P., and Delmer, D.** (2002). Sitosterol-beta-glucoside as primer for cellulose synthesis in plants. Science **295:** 147–150.

**Peng, L., Zhang, L., Cheng, X., Fan, L.S., and Hao, H.Q.** (2013). Disruption of cellulose synthesis by 2,6-dichlorobenzonitrile affects the structure of the cytoskeleton and cell wall construction in Arabidopsis. Plant Biol. (Stuttg.) **15:** 405–414.

**Robert, S., Bichet, A., Grandjean, O., Kierzkowski, D., Satiat-Jeunemaître, B., Pelletier, S., Hauser, M.T., Höfte, H., and Vernhettes, S.** (2005). An *Arabidopsis* endo-1,4-β-D-glucanase involved in cellulose synthesis undergoes regulated intracellular cycling. Plant Cell **17:** 3378–3389.

**Roelofsen, P.A.** (1965). Ultrastructure of the wall in growing cells and its relation to the direction of the growth. Adv. Bot. Res. **2:** 69–149.

**Roelofsen, P.A., and Houwink, A.L.** (1951). Cell wall structure of staminal hairs of *Tradescantia virginica* and its relation with growth. Protoplasma **40:** 1–22.

**Roelofsen, P.A., Dalitz, V.C., and Wijnman, C.F.** (1953). Constitution, submicroscopic structure and degree of crystallinity of the cell wall of *Halicystis osterhoutii*. Biochim. Biophys. Acta **11:** 344–352.

**Roland, J.C., Vian, B., and Reis, D.** (1975). Observations with cytochemistry and ultracryotomy on the fine structure of the expanding walls in actively elongating plant cells. J. Cell Sci. **19:** 239–259.

**Sato, S., et al**. (2001). Role of the putative membrane-bound endo-1,4-beta-glucanase KORRIGAN in cell elongation and cellulose synthesis in *Arabidopsis thaliana*. Plant Cell Physiol. **42:** 251–263.

**Scheible, W.R., Eshed, R., Richmond, T., Delmer, D., and Somerville, C.** (2001). Modifications of cellulose synthase confer resistance to isoxaben and thiazolidinone herbicides in Arabidopsis Ixr1 mutants. Proc. Natl. Acad. Sci. USA **98:** 10079–10084.

**Standal, R., Iversen, T.G., Coucheron, D.H., Fjaervik, E., Blatny, J.M., and Valla, S.** (1994). A new gene required for cellulose production and a gene encoding cellulolytic activity in *Acetobacter xylinum* are colocalized with the bcs operon. J. Bacteriol. **176:** 665–672.

**Szyjanowicz, P.M., McKinnon, I., Taylor, N.G., Gardiner, J., Jarvis, M.C., and Turner, S.R.** (2004). The irregular xylem 2 mutant is an allele of korrigan that affects the secondary cell wall of *Arabidopsis thaliana*. Plant J. **37:** 730–740.

**Thomas, L.H., Forsyth, V.T., Sturcová, A., Kennedy, C.J., May, R.P., Altaner, C.M., Apperley, D.C., Wess, T.J., and Jarvis, M.C.** (2013). Structure of cellulose microfibrils in primary cell walls from collenchyma. Plant Physiol. **161:** 465–476.

**Uemura, T., Ueda, T., Ohniwa, R.L., Nakano, A., Takeyasu, K., and Sato, M.H.** (2004). Systematic analysis of SNARE molecules in Arabidopsis: Dissection of the post-Golgi network in plant cells. Cell Struct. Funct. **29:** 49–65.

**Updegraff, D.M.** (1969). Semimicro determination of cellulose in biological materials. Anal. Biochem. **32:** 420–424.

**Urbanowicz, B.R., Bennett, A.B., Del Campillo, E., Catalá, C., Hayashi, T., Henrissat, B., Höfte, H., McQueen-Mason, S.J., Patterson, S.E., Shoseyov, O., Teeri, T.T., and Rose, J.K.C.** (2007). Structural organization and a standardized nomenclature for plant endo-1,4-β-glucanases (cellulases) of glycosyl hydrolase family 9. Plant Physiol. **144:** 1693–1696.

**Wyatt, S.E., and Carpita, N.C.** (1993). The plant cytoskeleton-cell-wall continuum. Trends Cell Biol. **3:** 413–417.

**Yoshida, K., Imaizumi, N., Kaneko, S., Kawagoe, Y., Tagiri, A., Tanaka, H., Nishitani, K., and Komae, K.** (2006). Carbohydrate-binding module of a rice endo-beta-1,4-glycanase, OsCel9A, expressed in auxin-induced lateral root primordia, is post-translationally truncated. Plant Cell Physiol. **47:** 1555–1571.

**Zhang, T., Mahgsoudy-Louyeh, S., Tittmann, B., and Cosgrove, D.J.** (2013). Visualization of the nanoscale pattern of recently-deposited cellulose microfibrils and matrix materials in never-dried primary walls of the onion epidermis. Cellulose **21:** 853–862.

**Zuo, J., Niu, Q.W., Nishizawa, N., Wu, Y., Kost, B., and Chua, N.H.** (2000). KORRIGAN, an *Arabidopsis* endo-1,4-β-glucanase, localizes to the cell plate by polarized targeting and is essential for cytokinesis. Plant Cell **12:** 1137–1152.